JACS
JOURNAL OF THE AMERICAN CHEMICAL SOCIETY
Article
pubs.acs.org/JACS

Series of Multifluorine Substituted Oligomers for Organic Solar Cells with Efficiency over 9% and Fill Factor of 0.77 by Combination Thermal and Solvent Vapor Annealing

Jin-Liang Wang,*[,†] Kai-Kai Liu,[†] Jun Yan,[‡] Zhuo Wu,[†] Feng Liu,*[,§] Fei Xiao,[†] Zheng-Feng Chang,[†] Hong-Bin Wu,*[,‡] Yong Cao,[‡] and Thomas P. Russell[§]

[†]Beijing Key Laboratory of Photoelectronic/Electrophotonic Conversion Materials, Key Laboratory of Cluster Science of Ministry of Education, School of Chemistry, Beijing Institute of Technology, 5 South Zhongguancun Street, Beijing 100081, China

[‡]Institute of Polymer Optoelectronic Materials and Devices, State Key Laboratory of Luminescent Materials and Devices, South China University of Technology, 381 Wushan Road, Guangzhou 510640, China

[§]Materials Science Division, Lawrence Berkeley National Lab, Berkeley, California 94720, United States

Supporting Information

ABSTRACT: We report the synthesis of a family of multifluorine substituted oligomers and the corresponding polymer that have the same backbones but different conjugation lengths and amounts of fluorine atoms on the backbone. The physical properties and photovoltaic performances of these materials were systematically investigated using optical absorption, charge mobility, atomic force microscopy, transmission electron microscopy, grazing incidence X-ray diffraction, resonant soft X-ray scattering methods, and photovoltaic devices. The power conversion efficiencies (PCEs) based on oligomers were much higher than that in the polymer. Moreover, the devices based on **BIT6F** and **BIT10F**, which have an axisymmetric electron-deficient difluorobenzothiadiazole as the central unit, gave slightly higher PCEs than those with centrosymmetric electron-rich indacenodithiophene (IDT) as the central unit (**BIT4F** or **BIT8F**). Using proper solvent vapor annealing (SVA), particularly using thermal annealing (TA) followed by SVA, the device performance could be significantly improved. Notably, the best PCE of 9.1% with a very high FF of 0.76 was achieved using the medium-sized oligomer **BIT6F** with the optimized film morphology. This efficiency is the highest value reported for organic solar cells from small-molecules without rhodanine terminal group. More excitingly, devices from the shortest oligomer **BIT4F** showed an impressively high FF of 0.77 (the highest FF value reported for solution-processed small-molecule organic solar cells). These results indicate that photovoltaic performances of oligomers can be modulated through successive change in chain-length and fluorine atoms, alternating spatial symmetric core, and combined post-treatments.

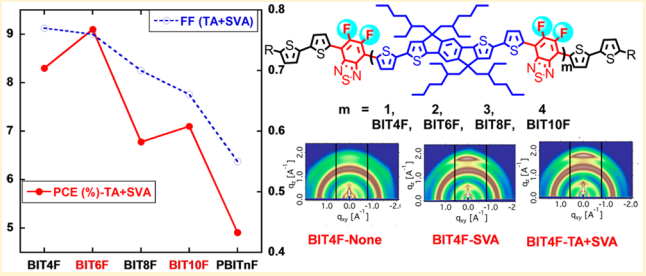

INTRODUCTION

Bulk-heterojunction organic solar cells (BHJ-OSCs) have been considered as a promising renewable and low-cost energy conversion technology owing to the advantages of light weight, solution processability, and flexibility.[1−8] In recent years, the power conversion efficiency (PCE) of BHJ-OSCs has been significantly improved through the synthesis of new photoactive and interfacial layer materials, optimization of film morphology, and the design of new device structures.[9−14] Currently, the design and synthesis of new conjugated polymers and oligomer donor materials is the key and the determining factor for device performance in BHJ-OSCs, although the building blocks used in high-performance oligomers and polymers are still very limited.[15−28] Small-molecules or oligomers, on the other hand, having better-defined chemical structures, are easier to purify, ensuring better reproducibility in device performance, and are more suitable to establish a structure−properties−device performance relationship in comparison with polymer counterparts.[29,30] Significant progress has been made with small-molecule organic solar cells and PCEs comparable to the best polymer solar cells have been achieved.[31−65] The performance of small-molecules that can deliver high PCE strongly depends on the core and end-capping units. For example, benzodithiophene or oligothiophene is often used as the core unit and rhodanine derivative as the terminal group for highly efficient (over 9% of PCE) small-molecule donor materials,[66−69] while the replacement of other core and terminal groups can usually lead to relatively low PCEs owing to their poor film quality and low fill factor, even upon careful device optimizations. Consequently, developing highly efficient and high fill factor conjugated small-molecule donor materials from novel core building blocks that are easy to synthesize is important in advancing the field.

Received: April 5, 2016
Published: May 26, 2016

DOI: 10.1021/jacs.6b03495
J. Am. Chem. Soc. 2016, 138, 7687−7697

Chart 1. Chemical Structures of Multifluorine Substituted Oligomers and Reference Polymer

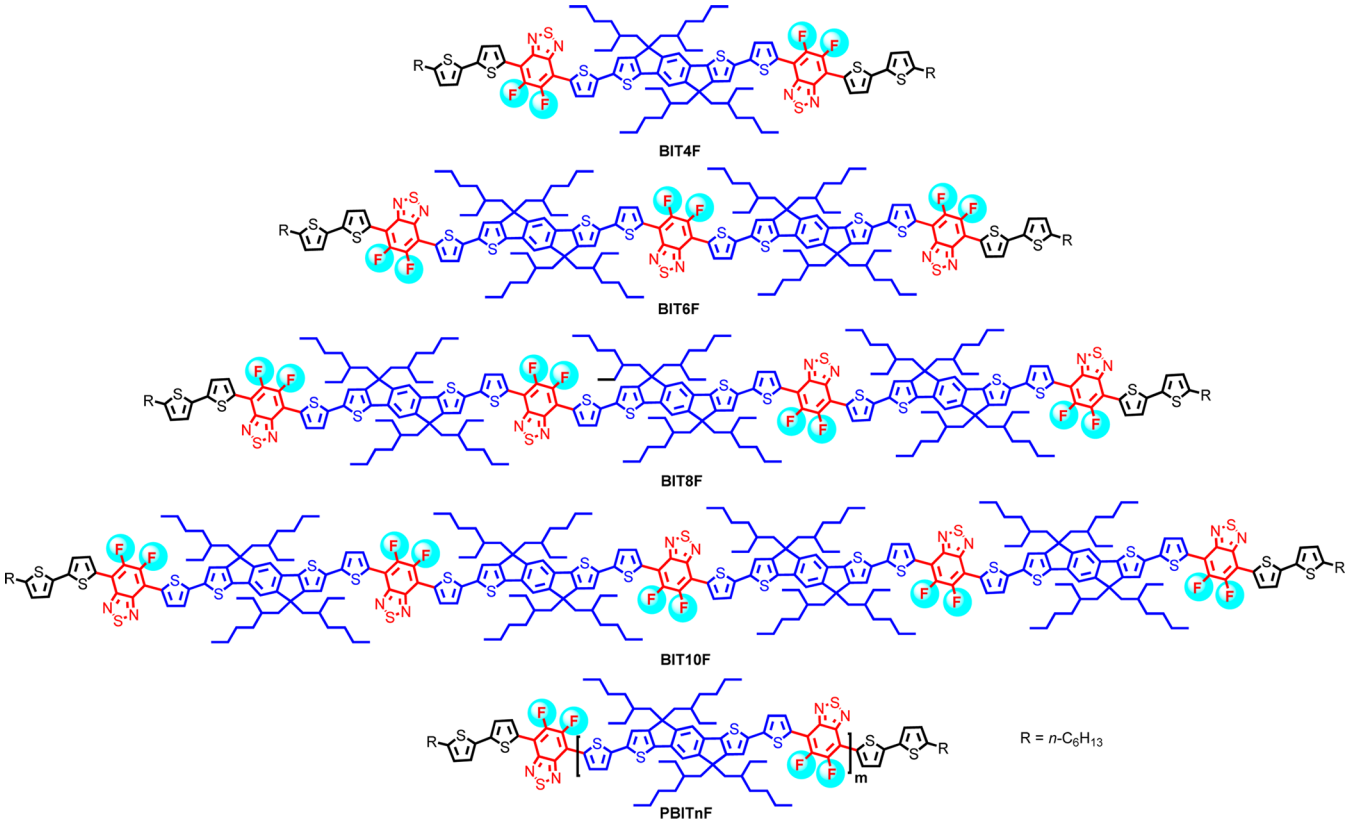

Table 1. Summary of the Device Performances and the Charge Carrier Mobilities from Blend Films of These Oligomers/Polymer and $PC_{71}BM$

oligomers/polymer	J_{sc} (mA/cm^2)	V_{oc} (V)	FF (%)	PCE_{av} (PCE_{max}) (%)	μ_e (cm^2 V^{-1} s^{-1})	μ_h (cm^2 V^{-1} s^{-1})	μ_e/μ_h ratio
BIT4F	10.86 ± 0.25	0.94 ± 0.01	60.61 ± 1.42	6.19 ± 0.09(6.20)	(1.63 ± 0.14) × 10^{-4}	(8.30 ± 0.73) × 10^{-6}	~19.60
BIT4F[a]	12.20 ± 0.21	0.89 ± 0.01	75.33 ± 0.39	8.16 ± 0.12(8.23)	(1.70 ± 0.16) × 10^{-4}	(4.49 ± 0.69) × 10^{-4}	~0.38
BIT4F[b]	12.25 ± 0.15	0.89 ± 0.01	76.30 ± 0.60	8.27 ± 0.10(8.35)	(1.81 ± 0.08) × 10^{-4}	(8.50 ± 0.91) × 10^{-4}	~0.21
BIT6F	11.61 ± 0.33	0.91 ± 0.01	60.19 ± 1.40	6.34 ± 0.20(6.66)	(5.93 ± 0.46) × 10^{-5}	(3.26 ± 0.27) × 10^{-6}	~18.20
BIT6F[a]	11.41 ± 0.06	0.89 ± 0.01	73.38 ± 1.29	7.63 ± 0.12(7.75)	(9.98 ± 0.22) × 10^{-5}	(9.77 ± 0.27) × 10^{-5}	~1.02
BIT6F[b]	12.97 ± 0.40	0.91 ± 0.01	73.11 ± 1.47	8.66 ± 0.15(8.80)	(1.06 ± 0.03) × 10^{-4}	(1.04 ± 0.05) × 10^{-4}	~1.02
BIT6F[c]	13.39 ± 0.15	0.89 ± 0.01	75.17 ± 0.58	8.91 ± 0.19(9.09)	(1.06 ± 0.03) × 10^{-4}	(1.04 ± 0.05) × 10^{-4}	~1.02
BIT8F	10.57 ± 0.46	0.88 ± 0.01	56.05 ± 3.40	5.23 ± 0.14(5.31)	(1.84 ± 0.65) × 10^{-5}	(1.34 ± 0.53) × 10^{-6}	~13.8
BIT8F[a]	10.29 ± 0.77	0.88 ± 0.01	65.38 ± 3.42	5.93 ± 0.19(5.96)	(1.00 ± 0.05) × 10^{-4}	(9.94 ± 0.71) × 10^{-4}	~1.01
BIT8F[b]	10.90 ± 0.16	0.89 ± 0.01	69.07 ± 0.82	6.67 ± 0.15(6.78)	(1.16 ± 0.05) × 10^{-4}	(2.27 ± 0.15) × 10^{-4}	~0.51
BIT10F	11.62 ± 0.24	0.92 ± 0.00	58.99 ± 0.23	6.30 ± 0.16(6.45)	(5.86 ± 0.44) × 10^{-5}	(3.05 ± 0.33) × 10^{-6}	~19.20
BIT10F[a]	11.38 ± 0.25	0.92 ± 0.00	61.30 ± 2.82	6.39 ± 0.18(6.55)	(8.16 ± 0.36) × 10^{-5}	(2.30 ± 0.31) × 10^{-5}	~3.55
BIT10F[b]	11.72 ± 0.08	0.91 ± 0.01	65.78 ± 0.67	7.04 ± 0.08(7.10)	(1.03 ± 0.04) × 10^{-4}	(2.81 ± 0.41) × 10^{-5}	~3.66
PBITnF	6.22 ± 0.39	0.87 ± 0.01	54.65 ± 1.48	2.96 ± 0.14(3.16)	(2.00 ± 0.08) × 10^{-5}	(2.75 ± 0.51) × 10^{-6}	~7.29
PBITnF[a]	5.76 ± 0.53	0.87 ± 0.01	57.65 ± 1.13	3.10 ± 0.34(3.45)	(2.15 ± 0.10) × 10^{-5}	(1.03 ± 0.10) × 10^{-5}	~2.09
PBITnF[b]	8.64 ± 0.98	0.89 ± 0.01	55.31 ± 0.83	4.23 ± 0.43(4.91)	(2.59 ± 0.20) × 10^{-5}	(1.11 ± 0.22) × 10^{-5}	~2.32

[a]With CH_2Cl_2 vapor annealing. [b]With thermal annealing and followed with CH_2Cl_2 vapor annealing. [c]With thermal annealing and followed with CH_2Cl_2 vapor annealing (the active area of the device is 3.2 mm^2). The average values are calculated from >10 devices with standard deviation for the measurements.

Recently, attempts have been made to take advantage of both small-molecules and polymers to synthesize a "medium-sized molecule" with extended D−A conjugation.[70−72] However, most of these materials have exhibited low fill factor due to poor morphologies and/or less than optimized charge transport properties in devices.[71,72] Comparative studies of oligomers with progressively increasing chain-lengths, and the corresponding polymer, provide an opportunity to investigate chain-length and performance relationship, which is an important topic in conjugated materials research. Meanwhile, the spatial symmetry and chemical constitution along with chain-length variation dictate molecular packing, phase separation, and device performance properties.[66,71,72]

It is well-known that fluorine substitution can decrease the HOMO energy level of the conjugated polymers.[73−80] Meanwhile, fluorine substitution also leads to rigid and planar backbone due to intramolecular hydrogen bonds. In practice, devices from fluorine substituted polymers usually show

DOI: 10.1021/jacs.6b03495
J. Am. Chem. Soc. 2016, 138, 7687−7697

Scheme 1. Synthesis of these Oligomers and Reference Polymer

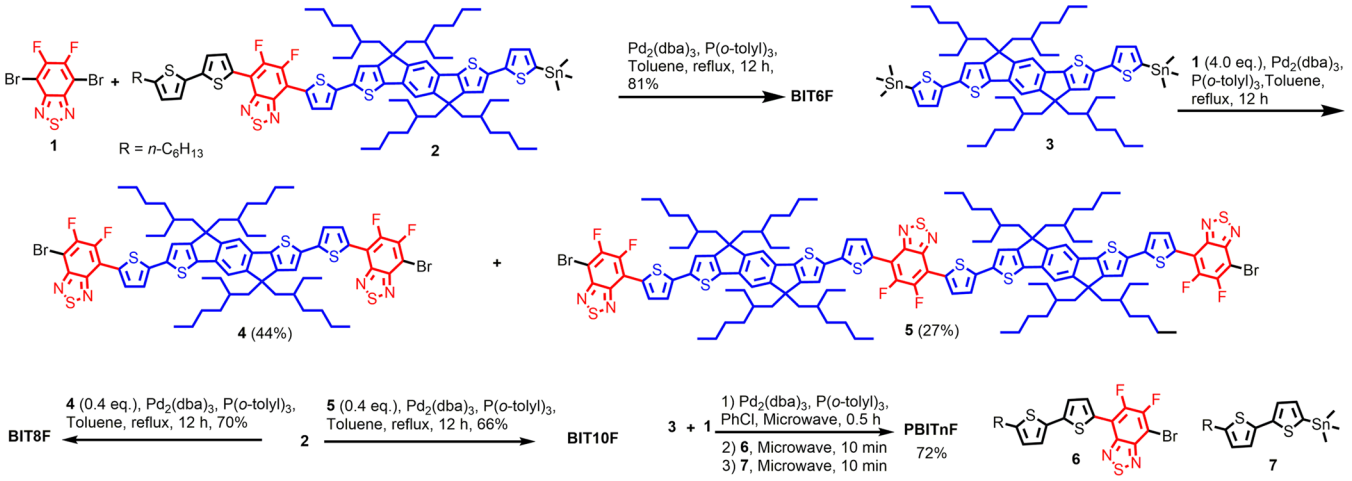

improved PCE.[73−80] However, due to the difficulty of the synthesis and a dearth of appropriate building blocks, studies incorporating multiple fluorine substituents ($n > 4$) in a series of small-molecules that have superior photovoltaic properties are really rare. Therefore, it would be of interest to systematically vary the fluorine content and the molecular symmetry of oligomer, so as to determine physical property and device performance changes.

To address these challenges, a family of linear donor−acceptor multifluorine substituted oligomers (**BIT4F**, **BIT6F**, **BIT8F**, and **BIT10F**) and the corresponding polymer, **PBITnF**, with an electron-rich indacenodithiophene (IDT) unit as the donor and an electron-deficient difluorobenzothiadiazoles unit as the acceptor were synthesized (Chart 1). The chain-length dependence of the band gap and the HOMO/LUMO energy levels in solution and the solid state, charge transport properties and the morphologies of blend films, and the photovoltaic properties of these IDT-difluorobenzothiadiazole-based oligomers were investigated (Table 1). These materials exhibit good solubility in chlorobenzene owing to the four 2-ethylhexyl chain substitutions on each IDT unit and two terminal hexyl groups and were solution-cast to form smooth films. The OPV devices based on the blends of these oligomers with $PC_{71}BM$ showed PCEs over 6.6%, which were remarkably higher than that of the corresponding polymer **PBITnF**. More importantly, the best PCE of 9.09% (with a V_{oc} of 0.89 V, a J_{sc} of 13.44 mA cm^{-2}, and a FF of 0.76) and average PCE of ca. 8.9% were achieved for these devices using **BIT6F** (with six fluorine atoms on the backbone and difluorobenzothiadiazole as the central unit):**$PC_{71}BM$** blends. To the best of our knowledge, this is the highest PCE of solution-processed BHJ solar cells based on small-molecules without a rhodanine as the terminal group, and is among the best value for small-molecule-based solar cells. Surprisingly, the devices from **BIT6F** or **BIT10F**, both having an axisymmetric, electron-deficient difluorobenzothiadiazoles center, gave slightly higher PCEs when compared to those of **BIT4F** or **BIT8F**, which have centrosymmetric electron-rich IDT central units. More interestingly, devices from the shortest oligomer **BIT4F** (with four fluorine atoms on the backbone) had an excellent FF of ca. 0.77, which is the highest FF value reported for solution-processed small-molecule organic solar cells. These results provide insights into understanding how OSC performance is influenced by alternating the spatial symmetry of the basic unit, the number of fluorine atoms, and the conjugation length of the backbone in a series of donor−acceptor oligomers.

RESULTS AND DISCUSSION

The synthetic routes to these oligomeric small-molecules, combining the advantages of divergent and convergent synthetic strategies, are presented in Scheme 1. **BIT6F** was prepared by a Stille coupling reaction between dibromide (**1**)[81] and monotin reagent **2**[57] (2.5 equiv) as a dark solid in 81% isolated yield. It was very challenging to efficiently synthesize the long oligomers **BIT8F** and **BIT10F** due to lack of the regioselectivity of the two bromide reaction sites of the symmetric dibromide **1**, which led to lowering the isolated yields of the monofunctionalized compound. The preparation of these key extended "core" species **4** and **5** was achieved by coupling ditin **3**[82] with excess dibromide **1** (4 equiv) by a Stille coupling reaction in 44% and 27% yields, respectively. Unreacted **1** could be recovered, and the polymerized species were quite low in yields (could not be fully separated) due to the high reactant ratio of **1** to **3**. Finally, **BIT8F** and **BIT10F** were obtained through Stille coupling reactions between monotin **2** and core **4** or **5** in 70% and 66% isolated yield, respectively. The reference polymer **PBITnF** was synthesized in 72% yield by a microwave assisted Stille coupling of **1** and **3** in chlorobenzene and then was followed with adding end-capping materials to remove reactive end groups. The polymer was purified by Soxhlet extraction with acetone, hexane, and finally chloroform. The chloroform fraction was collected and reprecipitated in methanol to afford the polymer **PBITnF** as a dark solid with M_n = 11.0 kDa using a PS/trichlorobenzene standard at high temperature. All oligomers were purified by silica gel column chromatography, and their structures and purity were fully characterized by ^{1}H and ^{13}C NMR spectroscopy, elemental analysis, and ESI/MALDI-TOF MS. Under N_2 atmosphere, the onset temperature with 5% weight-loss by thermogravimetric analysis (TGA) was over 390 °C for all oligomers and polymer (Figure S1), which demonstrated the good thermal stability of these oligomers/polymer.

The absorption spectra of these materials in diluted chloroform solutions and in thin films were shown in Figure 1. All molecules showed two distinct and intense absorption bands (band I, 300−500 nm; band II, 500−800 nm) with a high molar extinction coefficient coming from the $\pi-\pi^*$ transition of conjugated backbone and the intramolecular

DOI: 10.1021/jacs.6b03495
J. Am. Chem. Soc. 2016, 138, 7687−7697

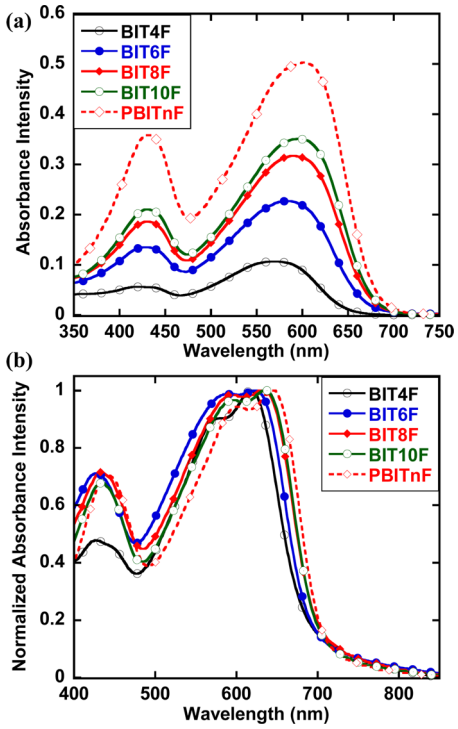

Figure 1. Absorption spectra of these oligomers and polymer (a) in chloroform solutions (1×10^{-6} M) and (b) in the thin films.

charge transfer (ICT). In solution, longer oligomer **BIT6F** showed an obvious red-shift in comparison with that of **BIT4F**. Moreover, the spectra of the longest oligomer **BIT10F** showed absorption peaks at 431 and 596 nm. These results indicated that chain extension led to a progressive red-shift of the absorption maximum (λ_{max}) with an increase of the molecular absorption coefficient. These features were also clearly apparent in the spectra of polymer **PBITnF**. The absorption spectra of these materials in films are red-shifted and showed enhanced 0−0 vibrational peak. In detail, thin films of **BIT4F**, **BIT6F**, **BIT8F**, **BIT10F**, and polymer **PBITnF** showed red-shifts of 49, 44, 45, 39, and 39 nm, respectively, in comparison to these absorption maxima in solutions. These features were generally interpreted as the higher π-electron delocalization and more planar conjugated backbone by interchain packing in the solid state. Moreover, **BIT4F** exhibited more obvious "aggregation"/0−0 vibrational peaks, which may relate to a stronger interchain aggregation. Optical band gaps of oligomers and polymer were estimated to be 1.81, 1.79, 1.78, 1.77, and 1.77 eV, respectively, from the absorption onsets of thin films. These results indicated that conjugation of **BIT10F** had essentially reached the effective conjugation length of the **PBITnF** polymer.

To estimate the energy level of these materials and understand the relationship between the chemical structure and the redox properties of the desired materials, the electrochemical properties of these materials were studied by cyclic voltammetry (CV). Thin films on Pt electrode were prepared and $Ag/AgNO_3$ (0.01 M in CH_3CN) was used as the reference electrode), As shown in Figure S2 and Table 2, the CV curves of thin films based on these materials showed one quasi-reversible oxidation and reduction wave. The highest occupied molecular orbitals (HOMOs) and lowest unoccupied molecular orbitals (LUMOs) energy levels were calculated from the onset oxidation curves and the onset reduction curves, and were −5.32 eV/−3.17 eV for **BIT6F**, −5.29 eV/−3.18 eV for **BIT8F**, −5.28 eV/−3.19 eV for **BIT10F**, and −5.27 eV/−3.22 eV for **PBITnF**, respectively. The HOMO energy level was slightly up-shifted with increasing chain length because of the more extended conjugation. Polymer PBITnF, on the other hand, showed the deepest LUMO energy levels due to the extended conjugation and highest content of difluorinated benzothiadiazole. The electrochemical bandgaps were slightly larger than the corresponding optical bandgaps due to difference in measurement methods.

Bulk-heterojunction cells using these oligomers as donors were fabricated using device structure of ITO/PEDOT:PSS/oligomer or polymer:**$PC_{71}BM$**/PFN/Al. By varying the D/A ratio in a broad range, the optimal donor/**$PC_{71}BM$** weight ratio was 1:2 for **BIT4F** and 1:3 for other oligomer and polymer. All of the devices based on our oligomers/polymer and **$PC_{71}BM$** without any treatment exhibited a high V_{oc} (ca. 0.9 V) (see Table 1 and Figure 2), consistent with their deep-lying HOMO energy levels. The **BIT6F**-based device without any treatment showed the highest PCE of 6.66% with a J_{sc} of 12.15 mA cm^{-2} and a high FF of 0.61. In contrast, the device based on a blend of **PBITnF**:**$PC_{71}BM$** only gave moderate PCE of 3.16% with a lowest J_{sc} of 6.82 mA cm^{-2} and a lowest FF of 0.53. Moreover, the devices based on **BIT6F** or **BIT10F** that had axisymmetric electron-deficient difluorobenzothiadiazoles centers gave slightly higher PCEs than those of the device from **BIT4F** or **BIT8F**, which had a centrosymmetric electron-rich IDT center unit, respectively. Indeed, the dependence of the photovoltaic performance on the conjugated chain-length highlights the importance of optimizing chain-length and fluorine numbers in the donor materials, which could be very effective in enhancing J_{sc} and FF without sacrificing the V_{oc}.

To fully exploit the potential of these oligomers, we further employ thermal annealing (TA) and solvent vapor annealing (SVA) treatments to control the active layer morphology and optimize device performance.[67,83−86] When CH_2Cl_2 vapor annealing (SVA) was used, the blend of the **BIT4F**/**$PC_{71}BM$** sample showed the highest PCE of 8.23% with the highest J_{sc} of 12.13 mA cm^{-2}, V_{oc} of 0.89 V, and highest FF of 0.76 (see Table 1). This is the highest improvement of PCE in this series. The best PCEs were found to be 7.75% for **BIT6F**/**$PC_{71}BM$** and 5.96% for the **BIT8F**/**$PC_{71}BM$** under SVA. The PCEs of

Table 2. Photophysical and Electrochemical Properties of Oligomers and Reference Polymer in Solutions and in Thin Films

compd	λ_{max}abs (sol) (nm)	λ_{max}abs (film) (nm)	$E_{ox(onset)}$[a] (V)	$E_{red(onset)}$[a] (V)	E_{HOMO} (eV)	E_{LUMO} (eV)	$E_{g(cv)}$ (eV)	$E_{g(opt)}$[b] (eV)
BIT4F	418, 569	426, 575, 618	0.53	−1.63	−5.33	−3.17	2.16	1.81
BIT6F	427, 583	432, 593, 627	0.52	−1.63	−5.32	−3.17	2.15	1.79
BIT8F	430, 590	433, 595, 635	0.49	−1.62	−5.29	−3.18	2.11	1.78
BIT10F	431, 596	435, 595, 635	0.48	−1.61	−5.28	−3.19	2.09	1.77
PBITnF	432, 601	434, 585, 640	0.47	−1.58	−5.27	−3.22	2.05	1.77

[a]Potentials are measured relative to a Fc/Fc^+ redox couple. [b]Estimated from the onset of thin-film absorption.

DOI: 10.1021/jacs.6b03495
J. Am. Chem. Soc. 2016, 138, 7687−7697

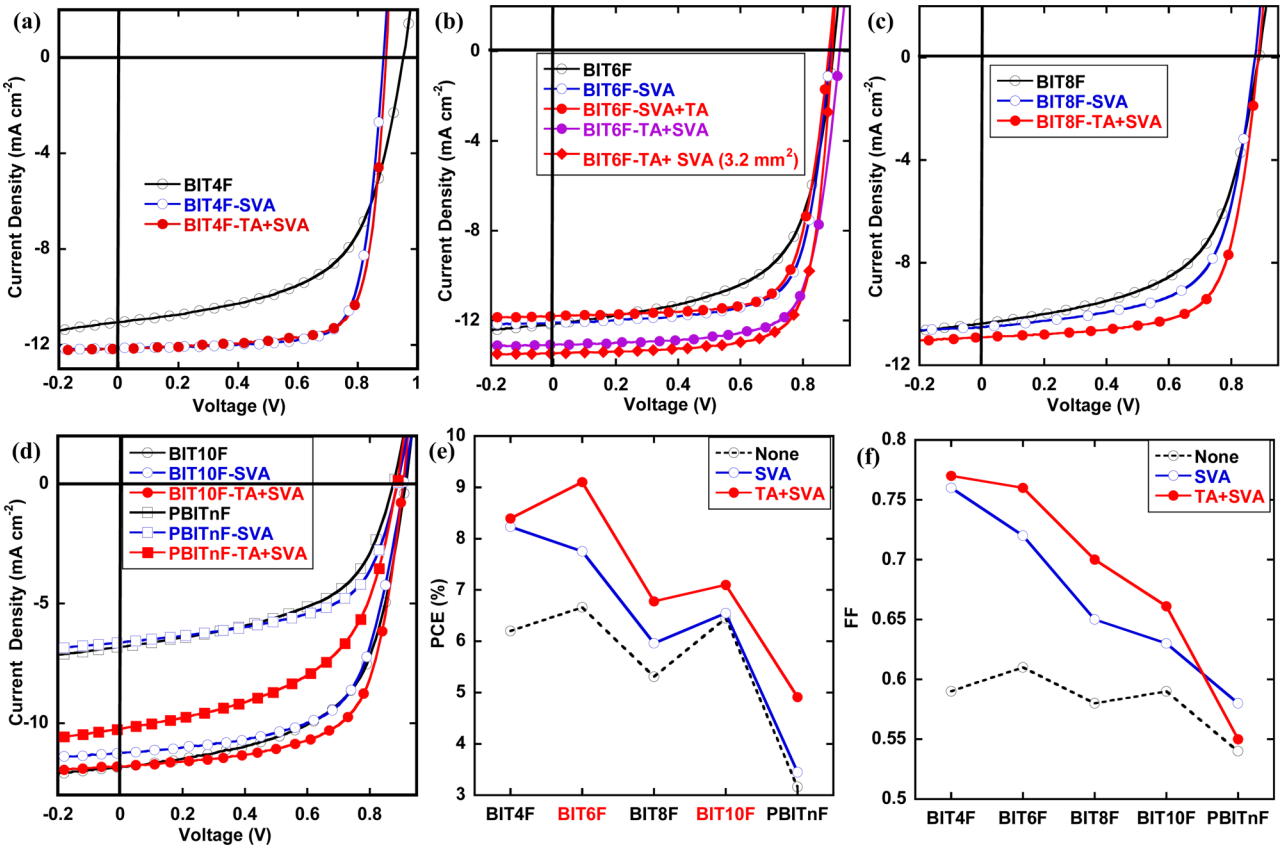

Figure 2. Characteristic current density vs voltage (J–V) curves (a–d) and plot of the PCE and FF variations (e, f) of the best OSC devices based on these oligomers/polymer and **PC$_{71}$BM** before/after treatment with CH_2Cl_2 vapor annealing or with a two-step annealing process.

devices based on the longest oligomer **BIT10F** and polymer **PBITnF** were only slightly enhanced after CH_2Cl_2 vapor annealing due to a lack of improvement in the FF. Previous reports indicate that solubility of the donor and acceptor materials in the vapor annealing solvent is critical for the improvement in photovoltaic performance.[83,86] It is worth noting that the increase of fluorine substitution led to a decrease in solubility due to the enhancement of interchain interactions.[70] As seen in our measurement, **BIT4F** with four fluorine atoms in one molecule can be dissolved in CH_2Cl_2 in an excess of 40 mg/mL at room temperature. Meanwhile, **BIT6F** with six fluorine atoms in one molecule can be dissolved in CH_2Cl_2 in about 25 mg/mL at room temperature. In contrast, **BIT10F** with 10 fluorine atoms has a solubility below 10 mg/mL at room temperature. Thus, CH_2Cl_2 vapor annealing can be more effective for the shorter oligomers with fewer fluorine atoms since vapor molecules could more favorably interact with shorter oligomers to provide enough mobility to improve the morphology.

With combined thermal and CH_2Cl_2 vapor annealing for 30 s, all of the devices obtained further enhancement in PCE (see Table 1). The optimization of active layer film thickness on the device performance was investigated and was presented in Table S1. For example, the optimal blend film thickness was about 100 nm for **BIT4F**/**PC$_{71}$BM** and about 80 nm for **BIT6F**/**PC$_{71}$BM**, respectively. For the **BIT4F** devices, the best PCE increased to 8.35%, and FF increased to an impressively high value of 0.77. It was the highest FF value reported for solution-processed small-molecular organic solar cells to date. PCE of **BIT6F**/**PC$_{71}$BM** devices was sharply improved to 8.80% (with a high J_{sc} of 13.06 mA cm^{-2}, a V_{oc} of 0.92 V, and a high FF of 0.73). PCEs of **BIT8F**, **BIT10F**, and **PBITnF** were increased to 6.78%, 7.10%, and 4.91%, respectively. In contrast to the good performance of oligomers, the PCE of the polymer was still the lowest value after combined TA and SVA treatments. However, the best PCE of **PBITnF** is higher than that of the best reported difluorobenzothiadiazole/IDT-based polymer.[90] Overall, **BIT6F**-based devices exhibited the best potential upon the combined TA and SVA treatment. These results clearly indicated that combined TA and SVA treatment was more effective for the medium oligomers with proper fluorine atoms. A well-defined mask with a smaller area of 3.2 mm^2 was also used to precisely define the effective area of the device in measurement. We obtained the best PCE of 9.09% (average PCE of 8.9%) with a J_{sc} of 13.44 mA cm^{-2}, a V_{oc} of 0.89 V, and a FF of 0.76 from **BIT6F**/**PC$_{71}$BM** blends. The sequence of annealing, using SVA followed by TA, was also investigated on **BIT6F**/**PC$_{71}$BM** blends. The device gave performances similar to a single SVA treatment. This was because SVA was far more efficient in driving the morphology evolution than TA; thus subsequently TA did not help. To the best of our knowledge, the high efficiency of ca. 9.1% with high FF is among the best PCE in small-molecule OSCs. Furthermore, such outstanding efficiency is the highest value reported so far for small-molecules without rhodanine terminal group. Meanwhile, the current PCE is higher than the best reported values for difluorobenzothiadiazole/IDT-based small-molecules and polymers.[87−92]

The difference in physical and device performance change upon post-treatment for different oligomers is currently not

DOI: 10.1021/jacs.6b03495
J. Am. Chem. Soc. 2016, 138, 7687−7697

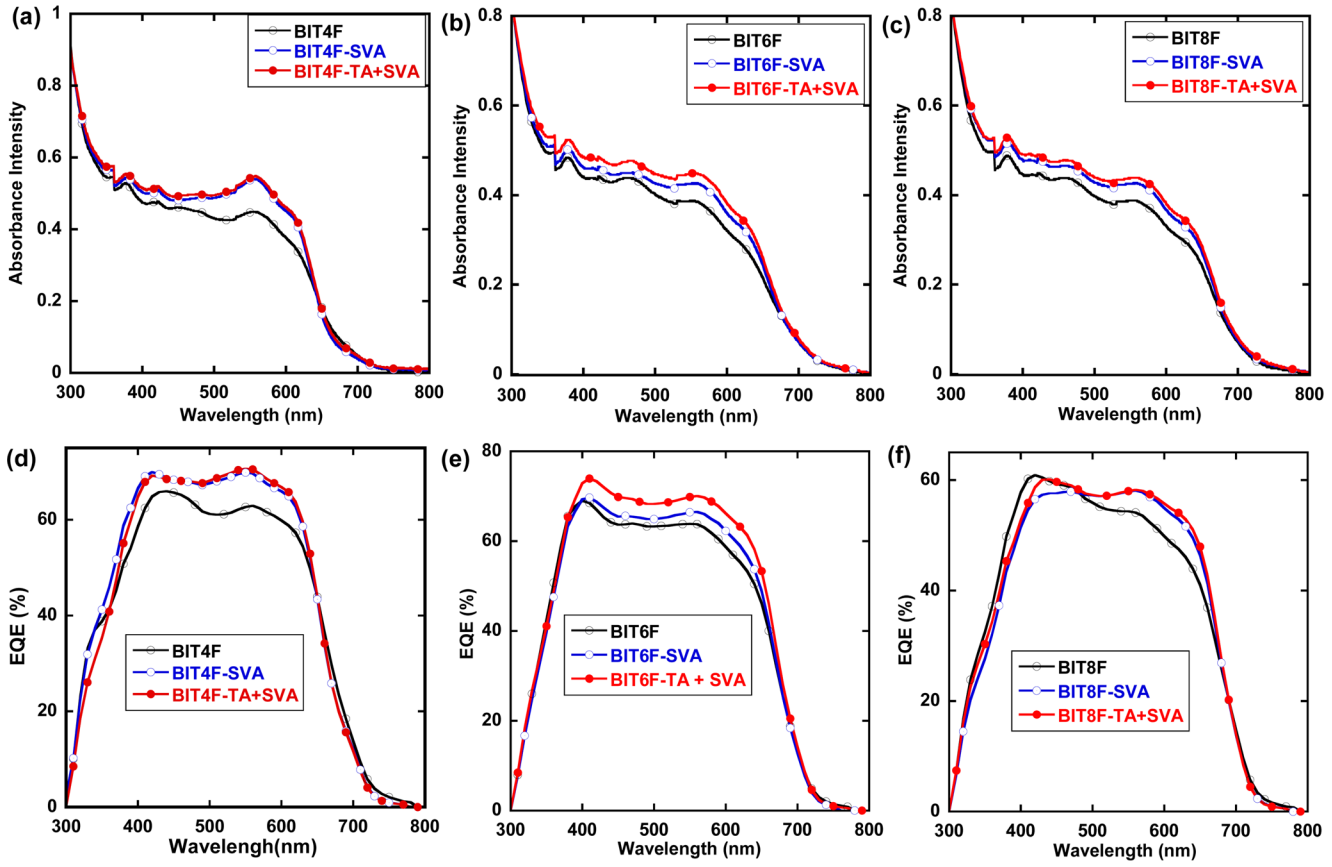

Figure 3. Absorption spectra (a–c) and corresponding EQE curves (d–f) of the best OSC devices of (a, d) **BIT4F**:$PC_{71}BM$ blend films, (b, e) **BIT6F**:$PC_{71}BM$ blend films, and (c, f) **BIT8F**:$PC_{71}BM$ blend films before/after treatment with CH_2Cl_2 vapor annealing or with the two-step annealing process. All of the integrated current density from the EQE curve agrees well with the J_{sc} value from the J–V curve.

clear. This should be related to chemical structure, molecular symmetry, and morphology and carrier dynamic factors. Thus, TA and SVA annealing effects were studied by UV–vis absorption spectra and external quantum efficiency (EQE) measurements to see the origin of the J_{sc} increase. As shown in Figure 3, solvent vapor annealed samples based on oligomers exhibited higher absorption intensity in 500–700 nm region when compared to as-cast thin films. Moreover, upon TA and the subsequent SVA, an obvious increase in the absorption intensity was observed in the **BIT6F**:$PC_{71}BM$ film. This effect was less pronounced in **BIT4F**, **BIT8F**, and **BIT10F** blends. These results indicated that both solvent vapor annealing and the two-step annealing treatment can lead to enhanced donor/acceptor molecular interaction and crystalline order in blend films. Thus, in a comparison with as-cast blend films, an enhancement in absorption intensity can be clearly seen. These features corresponded well with EQE responses (Figure 3), leading to J_{sc} improvement. Taking the **BIT6F** device for example, the EQE showed a maximal value of 74% at 410 nm and >65% over a broad wavelength range between 380 and 600 nm.

In addition to the change in absorption, the change in the film morphology was also important for the enhancement in photocurrent. We carried out atomic force microscopy (AFM), transmission electron microscopy (TEM), grazing incident X-ray diffraction (GIXD), and resonant soft X-ray scattering (RSoXS) to thoroughly investigate thin-film morphology. First, the surface morphology of the photoactive layers was studied by tapping mode AFM. Figure 4 and Figures S4–S7 showed

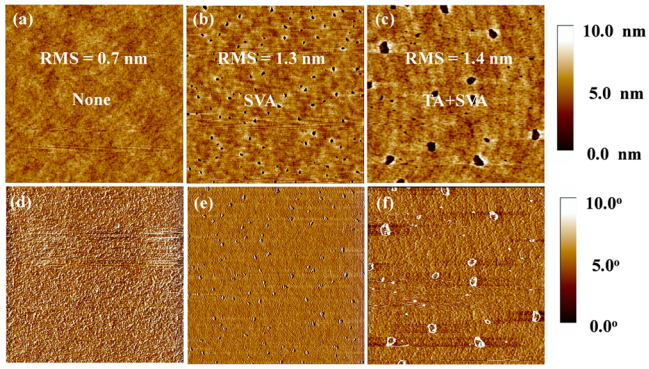

Figure 4. Tapping mode AFM height (a–c) and phase (d–f) images of 5 × 5 μm^2 portions of a blend film: (a, c) **BIT6F**/$PC_{71}BM$; (b, d) **BIT6F**/$PC_{71}BM$ after CH_2Cl_2 vapor annealing; (c, f) **BIT6F**/$PC_{71}BM$ after thermal annealing and followed with CH_2Cl_2 vapor annealing.

the height and phase images for the as-cast, SVA, and TA + SVA films. For the as-cast film, a smooth surface with a small root-mean-square (RMS) roughness (0.5–1.2 nm) was clearly seen. Upon SVA and TA + SVA, the RMS of the**BIT6F**:$PC_{71}BM$ film slightly increased from 0.8 nm (as-cast) to 1.3 and 1.4 nm, respectively, which was similar to that of a previous report.[86] Similarly, the RMS of blend films of other oligomers with $PC_{71}BM$ increased slightly after the treatments. In contrast, polymer thin films displayed a much larger domain size, which was responsible for the low value of

DOI: 10.1021/jacs.6b03495
J. Am. Chem. Soc. 2016, 138, 7687–7697

J_{sc}. The obvious differences in the surface morphology suggest that exciton diffusion and separation in the oligomer blend films are more efficient than in the polymer.

High-resolution TEM was used to monitor the interior morphology of the BHJ thin film (Figure 5 and Figure S8).

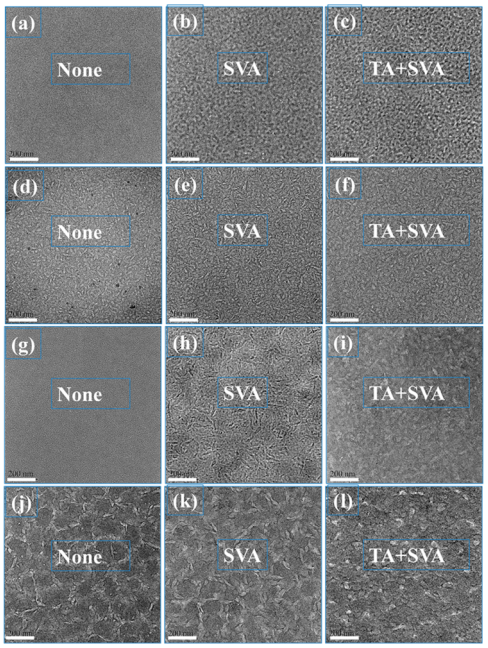

Figure 5. TEM images of blend films based on **BIT4F/PC_{71}BM** before and after annealing treatments (a–c); **BIT6F/PC_{71}BM** before and after annealing treatments (d–f); **BIT8F/PC_{71}BM** before and after annealing treatment (g–i); **BIT10F/PC_{71}BM** before and after annealing treatments (j–l).The scale bar is 200 nm.

BIT4F, **BIT6F**, and **BIT8F** blends exhibited a homogeneous morphology. When these films were exposed to CH_2Cl_2 vapor, a detailed morphology was found. The length scale of phase separation increased when the oligomer size increased. Upon combined thermal and solvent vapor annealing treatment, a similar or slightly enlarged length scale of phase separation was seen for **BIT4F** and **BIT6F** samples. Domain sizes grew much larger for the **BIT8F** sample. **BIT10F** blends showed quite a different morphology. A large scale phase separation was observed in the as-cast thin film. SVA treatment did not significantly change the morphology. TA plus SVA treatment led to a slightly more uniform TEM image, indicating that TA processs could be beneficial in driving better bicontinuous morphology, thus giving rise to a slightly increased FF and PCE, keeping with the small enhancement of PCE on post-treated samples. Changes of the interior morphology in oligomer blends after annealing treatments, in particular, for **BIT4F, BIT6F** and **BIT8F** samples, are beneficial for exciton diffusion/dissociation at the D/A interface and charge transport along the interpenetrating networks, which led to an increased J_{sc} and FF.[93,94] However, the polymer-based pristine blends displayed severe **PC_{71}BM**-rich aggregation on the 100–120 nm size scale. Thus, in the polymeric case, efficiency of excitons splitting would be low, and charge carrier transport would be less efficient.

Grazing incidence X-ray diffractions (GIXD) were used to investigate crystalline morphology of oligomers in BHJ blends. Figure 6a shows the 2-D diffraction images from which the crystalline structure and crystal orientation could be assessed. Figure 6b shows the in-plane and out-of-plane line cut profiles. This new family of oligomer donors showed a predominant "face-on" crystalline orientation, as shown by the strong (100) diffraction in the in-plane direction and $\pi-\pi$ stacking ((010) diffraction) in the out-of-plane direction. As-cast thin film showed weak (010) and (100) diffraction peaks, especially for the **BIT4F/PC_{71}BM** blend and **BIT6F/PC_{71}BM** blend. On the other side, upon SVA or combined TA and SVA treatments, the crystalline content of the film was found to be enhanced by the better defined scattering peak and intensities. The corresponding (100) and (010) peak information, the corresponding stacking distances, and the crystal sizes were summarized in Table S1. In as-cast **BIT4F/PC_{71}BM** and **BIT6F/PC_{71}BM** blends, the (100) diffraction in-plane direction was located at 0.26 and 0.31 $Å^{-1}$, giving a packing distance of 2.39 and 2.04 nm, respectively, corresponding to the alkyl-to-alkyl spacing in molecular crystals. The crystal coherence length (CCL) was estimated to be 5.98 and 29.32 nm by Scherrer equation, respectively. In addition, the **BIT4F/PC_{71}BM** and **BIT6F/PC_{71}BM** as-cast films showed a weak (010) diffraction at ca. 1.81 and 1.88 $Å^{-1}$ in out-of-plane direction, corresponding to $\pi-\pi$ stacking distances of 3.46 and 3.34 Å. The latter $\pi-\pi$ stacking distance was quite small as compared to those of many reported polymers and small-molecules. Such short $\pi-\pi$ stacking distances between small-molecule backbones suggested strong intermolecular interactions, which could promote highly efficient charge transport and lead to higher FF. The $\pi-\pi$ stacking peak coherence length was about 1.31 and 1.61 nm. It should be noted that the azimuthal spreading of $\pi-\pi$ stacking was obvious, covering a larger angle region (admittedly that higher intensity was concentrated in out-of-plane direction), and thus transport could be facilitated in all directions. Solvent vapor annealing led to strong enhancement in crystalline order in the blended films, as seen from the enhanced diffraction intensities of both the (100) diffraction peak in the in-plane direction and the (010) diffraction in the out-of-plane direction. In **BIT4F/PC_{71}BM** blends, (100) crystal size and the $\pi-\pi$ stacking peak coherence length increased to values of 26.79 and 2.93 nm, respectively. The (100) crystal size and the $\pi-\pi$ stacking peak coherence length for **BIT6F/PC_{71}BM** blends increased to values of 30.42 and 1.80 nm, respectively. These results indicated the SVA process promoted the mobility of donor molecules; thus, nucleation and growth led to more crystalline content and enlarged crystal size. Combined TA and SVA treatment led to even better crystal sizes and diffraction intensities in both (100) and $\pi-\pi$ stacking directions. It thus can be concluded that combined thermal and solvent vapor annealing are more effective in optimizing crystalline morphology in BHJ blends, which lead to enhanced charge carrier transport and charge collections. These results corresponded to the higher PCE and FF in solar cell devices.

Resonant soft X-ray scattering (RSoXS) was used to investigate the length scale of phase separation in the blended films. Scattering profiles of BHJ thin films based on oligomers and polymer processed from different conditions are shown in Figure 7 and Figure S9. For the as-cast thin film based on **BIT4F/PC_{71}BM**, the scattering profile showed a weak intensity in the high q region (>0.01 $Å^{-1}$); thus, a less defined nanomorphology existed in this sample. Thus, an inferior performance in solar cells would be expected. When solvent vapor annealing was used, a quick growth in scattering showed

DOI: 10.1021/jacs.6b03495
J. Am. Chem. Soc. 2016, 138, 7687–7697

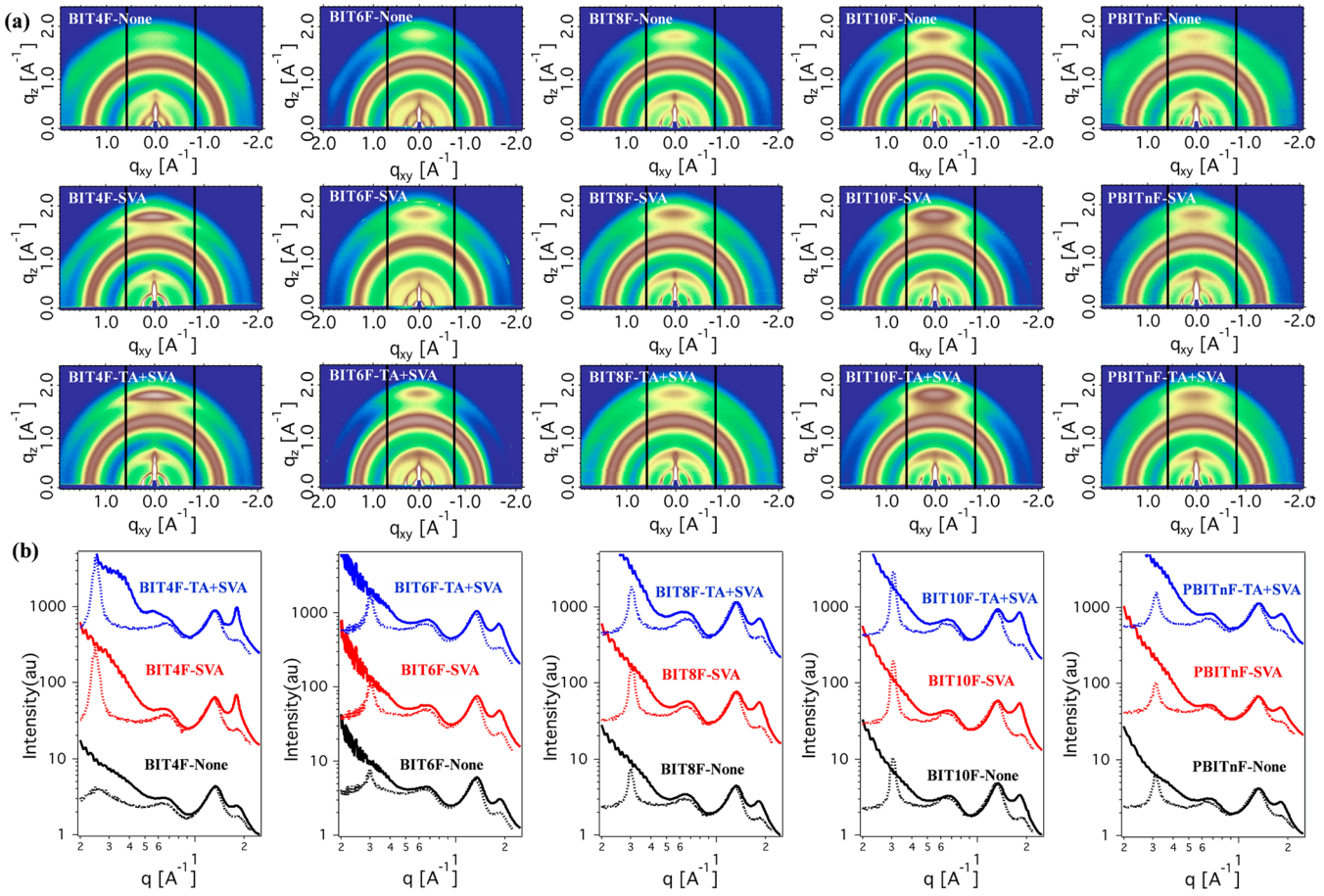

Figure 6. (a) GIXD pattern for the blend films based on oligomers/polymer with $PC_{71}BM$ before and after annealing treatments. (b) Out-of-plane (solid line) and in-plane (dotted line) line-cut profiles of the GIXD pattern for the blend films based on oligomers/polymer with $PC_{71}BM$ before and after annealing treatments.

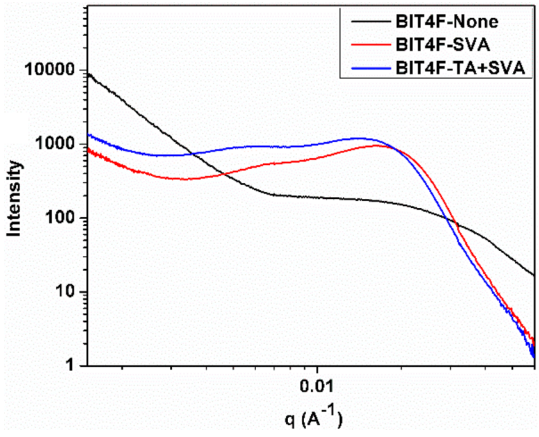

Figure 7. RSoXS profiles of **BIT4F/$PC_{71}BM$** blend films before and after annealing treatments.

up at 0.016 $Å^{-1}$. This peak corresponded to a 39 nm length scale of phase separation; TA + SVA treatment shifted the characteristic length scale to 42 nm. The well-defined scattering peak in a high q region defined a refined mesh network in the BHJ blends; thus, exciton splitting and charge transport can be facilitated. For these annealed samples, another feature appeared at ∼0.006 $Å^{-1}$, corresponding to a ∼100 nm morphology feature. Thus, in BHJ blends, the morphology is multilength scale. A 0.015 $Å^{-1}$ scattering peak was seen for **BIT6F/$PC_{71}BM$** blends after SVA treatment; in TA + SVA treatment, the scattering peak slight shifted to 0.017 $Å^{-1}$ (Supporting Information). The size scale of phase separations was slightly smaller than **BIT4F/$PC_{71}BM$** blended samples after TA + SVA treatment. Thus, superior performances were recorded in **BIT6F/$PC_{71}BM$** blends. The combined investigation of GIXD and RSoXS showed the physical nature of these oligomer blends under different processing conditions. The low crystalline content and weak phase separation in the as-cast sample indicated a good mixing of donor−acceptor components. SVA or TA + SVA processing allowed the molecules to move and order; thus, crystallization and phase separation changed. These observations are similar to the previously reported mechanistic understanding of SVA in tuning the morphology of BHJ blends.[83,95] Also, in our current case, a more detailed chemical variation of chain-length and molecular symmetries was employed to add to our understanding as to how to relate chemical structure change to morphology differences.[96] However, the **BIT8F/$PC_{71}BM$**-, **BIT10F/$PC_{71}BM$**-, and **PBITnF/$PC_{71}BM$**-based blends showed quite different morphologies. For these pristine blend films, a strong scattering peak was seen at ca. 0.0036 $Å^{-1}$, giving a distance of 170−180 nm. Solvent vapor annealing or dual TA and SVA treatment just slightly deceased or maintained the length scale of phase separation. Such a large length scale of phase separation, particularly for the **PBITnF/$PC_{71}BM$**-based

DOI: 10.1021/jacs.6b03495
J. Am. Chem. Soc. 2016, 138, 7687−7697

blends, is not favorable for exciton dissociation, and thus, a poor device performance is expected.

The influence of the chain-length of these oligomers, SVA treatment, and the combined treatment on the charge transport properties was studied by charge mobility measurements using a space charge limited current (SCLC) model. The structures of hole-only and electron-only devices were ITO/PEDOT/oligomers or polymer:**$PC_{71}BM$**/MoO_3/Al and ITO/ZnO/PFN/oligomers or polymer:**$PC_{71}BM$**/Ca/Al, respectively. Table 1 summarized the hole and electron mobilities deduced from the SCLC model, and the corresponding $J-V$ curves were shown in Figures S10−14. The **BIT4F**:**$PC_{71}BM$** film had the highest hole mobility among all of the materials in this study, mainly due to a relatively higher degree of molecular ordering. Moreover, the hole mobilities of all of devices (from the oligomers and polymer) increased about 1 order of magnitude after the SVA treatment or the combined TA and SVA treatment. Additionally, most devices with combined TA and SVA treatment exhibited higher hole mobilities than those using only an SVA treatment. The hole mobilities of **BIT4F**, **BIT6F**, and **BIT8F** were enhanced to $(8.50 \pm 0.91) \times 10^{-4}$ cm^2 V^{-1} s^{-1}, $(1.04 \pm 0.05) \times 10^{-4}$ cm^2 V^{-1} s^{-1}, and $(2.27 \pm 0.15) \times 10^{-4}$ cm^2 V^{-1} s^{-1} after the combined TA and SVA treatments, respectively, which were obviously higher than those of corresponding devices based on **BIT10F** and **PBITnF**. As for the electron mobility (μ_e) of devices, a slight increase was observed after the treatments. For example, the μ_e value of **BIT6F**/**$PC_{71}BM$** increased from $(5.93 \pm 0.46) \times 10^{-5}$ cm^2 V^{-1} s^{-1} to $(1.06 \pm 0.03) \times 10^{-4}$ cm^2 V^{-1} s^{-1} after the combined TA and SVA treatment. However, even after the combined TA and SVA treatment, the μ_e of the **PBITnF**/**$PC_{71}BM$** was found to be much lower than those in devices based on oligomers. This could be due to the severe **$PC_{71}BM$** aggregation and larger phase separation (as seen from morphological characterization) in the blended film that disrupt the electron transport channels. Nevertheless, the imbalance between the hole and electron mobility was dramatically improved after the treatments. For example, the ratios between the electron mobility and hole mobility (μ_e/μ_h) decreased from ca. 18.2 to 1.0 for **BIT6F**/**$PC_{71}BM$** after only an SVA treatment. This balance in charge transport is also maintained when the combined TA and SVA treatment was used. As a result of the improved charge transport properties, most of the photogenerated charge carriers can be readily collected at the electrode, as evidenced by the high FF (ca. 0.7) in the devices with proper treatment, which is particularly true for those devices based on **BIT4F** or **BIT6F**. It is worth noting that a high FF of 0.77 for the **BIT4F**-based devices is the highest FF value reported in the literature for solution-processed small-molecule organic solar cells. The much lower FF in all of the devices from **PBITnF** indicated that there are recombination loss pathways during the charge generation and/or transport process, thus preventing further enhancement. Overall, we attribute the single SVA treatment or combined TA and SVA treatment to be the main reason for the remarkable improvement of the FF as a result of much better charge transport and less charge recombination loss.[97−100]

CONCLUSION

In summary, a series of IDT-difluorobenzothiadiazole-based D−A oligomers with different spatial symmetry core units, different conjugation lengths, and different amounts of electronegative fluorine atoms (4, 6, 8, and 10 fluorine substituted backbone, respectively) as well as the corresponding polymer **PBITnF** were synthesized and systematically studied. The change of chain-length and spatial symmetry provided important parameters to tune energy levels, charge transport, and the morphology of the blended thin film, which had significant impact on the device performance. In comparison to the PCEs of the pristine devices, the best PCEs and fill factors based on all oligomers exhibited obvious enhancement upon solvent vapor annealing or combined thermal and solvent vapor annealing. Higher PCEs found for **BIT6F** and **BIT10F**, which have axisymmetric electron-deficient difluorobenzothiadiazole core units, were quite different from those of **BIT4F** and **BIT8F** (centrosymmetric electron-rich IDT core unit). Notably, the medium-sized oligomer **BIT6F** exhibited an outstanding PCE of 9.1% in a simple device configuration. This is the highest PCE of solution-processed BHJ solar cells based on small-molecules without a rhodanine as the terminal group reported to date, and is among one of the best small-molecule donor materials in single-junction solar cells. More importantly, we demonstrated that shortest oligomer **BIT4F**/**$PC_{71}BM$**-based devices after combined TA and SVA treatment had an extremely high FF of 77%, which is the highest FF value reported in the literature for solution-processed small-molecule organic solar cells. These oligomers/polymer design rationales (conjugation extension, variation of amounts of fluorine atoms, combined thermal and solvent vapor annealing) demonstrated here provide an effective approach to tune the energy levels and morphology of small-molecule donors that could be adopted to dramatically increase the PCE.

ASSOCIATED CONTENT

Supporting Information

The Supporting Information is available free of charge on the ACS Publications website at DOI: 10.1021/jacs.6b03495.

Synthesis and characterization of these oligomers/polymer, additional experimental results, and ^1H NMR and ^{13}C NMR spectra (PDF)

AUTHOR INFORMATION

Corresponding Authors

*jinlwang@bit.edu.cn
*iamfengliu@gmail.com
*hbwu@scut.edu.cn

Author Contributions

J.-L.W., K.-K.L., and J.Y. contributed equally.

Notes

The authors declare no competing financial interest.

ACKNOWLEDGMENTS

This work was financially supported by grants from the National Natural Science Foundation of China (No. 21472012, 21202007, 51225301, 91333206, 51521002); the Thousand Youth Talents Plan of China; Beijing Natural Science Foundation (2152027). F.L. and T.P.R. were supported by the U.S. Office of Naval Research under Contract N00014-15-1-2244 and the DOE, Office of Science, and Office of Basic Energy Sciences. The authors thank Dr. Jinhu Dou and Prof. Jian Pei (Peking University) for the helping on the high temperature gel permeation chromatography (GPC) experiment.

DOI: 10.1021/jacs.6b03495
J. Am. Chem. Soc. 2016, 138, 7687−7697

REFERENCES

(1) Beaujuge, P. M.; Fréchet, J. M. J. *J. Am. Chem. Soc.* **2011**, *133*, 20009−20029.
(2) Dennler, G.; Scharber, M. C.; Brabec, C. J. *Adv. Mater.* **2009**, *21*, 1323−1328.
(3) Inganäs, O.; Zhang, F.; Andersson, M. R. *Acc. Chem. Res.* **2009**, *42*, 1731−1739.
(4) Li, Y. *Acc. Chem. Res.* **2012**, *45*, 723−733.
(5) Zhou, H.; Yang, L.; You, W. *Macromolecules* **2012**, *45*, 607−632.
(6) Ye, L.; Zhang, S.; Huo, L.; Zhang, M.; Hou, J. *Acc. Chem. Res.* **2014**, *47*, 1595−1603.
(7) Chen, H.-Y.; Hou, J.; Zhang, S.; Liang, Y.; Yang, G.; Yang, Y.; Yu, L.; Wu, Y.; Li, G. *Nat. Photonics* **2009**, *3*, 649−653.
(8) Li, C.; Liu, M.; Pschirer, N.; Baumgarten, M.; Müllen, K. *Chem. Rev.* **2010**, *110*, 6817−6855.
(9) Price, S.; Stuart, A.; Yang, L.; Zhou, H.; You, W. *J. Am. Chem. Soc.* **2011**, *133*, 4625−4631.
(10) Wang, M.; Hu, X.; Liu, P.; Li, W.; Gong, X.; Huang, F.; Cao, Y. *J. Am. Chem. Soc.* **2011**, *133*, 9638−9641.
(11) Guo, X.; Zhou, N.; Lou, S. J.; Hennek, J. W.; Ortiz, R. P.; Butler, M. R.; Boudreault, P.-L.; Strzalka, J.; Morin, P.-O.; Leclerc, M.; Navarrete, J. T. L.; Ratner, M. A.; Chen, L. X.; Chang, R. P. H.; Facchetti, A.; Marks, T. J. *J. Am. Chem. Soc.* **2012**, *134*, 18427−18439.
(12) Cabanetos, C.; El Labban, A.; Bartelt, J. A.; Douglas, J. D.; Mateker, W. R.; Fréchet, J. M. J.; McGehee, M. D.; Beaujuge, P. M. *J. Am. Chem. Soc.* **2013**, *135*, 4656−4659.
(13) Osaka, I.; Kakara, T.; Takemura, N.; Koganezawa, T.; Takimiya, K. *J. Am. Chem. Soc.* **2013**, *135*, 8834−8344.
(14) Li, K.; Li, Z.; Feng, K.; Xu, X.; Wang, L.; Peng, Q. *J. Am. Chem. Soc.* **2013**, *135*, 13549−13557.
(15) Li, W.; Hendriks, K. H.; Furlan, A.; Wienk, M. M.; Janssen, R. A. J. *J. Am. Chem. Soc.* **2015**, *137*, 2231−2234.
(16) Qin, T.; Zajaczkowski, W.; Pisula, W.; Baumgarten, M.; Chen, M.; Gao, M.; Wilson, G.; Easton, C. D.; Müllen, K.; Watkins, S. E. *J. Am. Chem. Soc.* **2014**, *136*, 6049−6055.
(17) He, Z.; Xiao, B.; Liu, F.; Wu, H.; Yang, Y.; Xiao, S.; Wang, C.; Russell, T. P.; Cao, Y. *Nat. Photonics* **2015**, *9*, 174−179.
(18) Liu, Y.; Zhao, J.; Li, Z.; Mu, C.; Ma, W.; Hu, H.; Jiang, K.; Lin, H.; Ade, H.; Yan, H. *Nat. Commun.* **2014**, *5*, 5293.
(19) Ye, L.; Zhang, S.; Zhao, W.; Yao, H.; Hou, J. *Chem. Mater.* **2014**, *26*, 3603−3605.
(20) Chen, C.-C.; Chang, W.-H.; Yoshimura, K.; Ohya, K.; You, J.; Gao, J.; Hong, Z.; Yang, Y. *Adv. Mater.* **2014**, *26*, 5670−5677.
(21) Subbiah, J.; Purushothaman, B.; Chen, M.; Qin, T.; Gao, M.; Vak, D.; Scholes, F. H.; Chen, X.; Watkins, S. E.; Wilson, G. J.; Holmes, A. B.; Wong, W. W. H.; Jones, D. J. *Adv. Mater.* **2015**, *27*, 702−705.
(22) Huo, L.; Liu, T.; Sun, X.; Cai, Y.; Heeger, A. J.; Sun, Y. *Adv. Mater.* **2015**, *27*, 2938−2944.
(23) Zhang, J.; Zhang, Y.; Fang, J.; Lu, K.; Wang, Z.; Ma, W.; Wei, Z. *J. Am. Chem. Soc.* **2015**, *137*, 8176−8183.
(24) Mishra, A.; Bauerle, P. *Angew. Chem., Int. Ed.* **2012**, *51*, 2020−2067.
(25) Lin, Y.; Li, Y.; Zhan, X. *Chem. Soc. Rev.* **2012**, *41*, 4245−4272.
(26) Chen, Y.; Wan, X.; Long, G. *Acc. Chem. Res.* **2013**, *46*, 2645−2655.
(27) Coughlin, J. E.; Henson, Z. B.; Welch, G. C.; Bazan, G. C. *Acc. Chem. Res.* **2014**, *47*, 257−270.
(28) Roncali, J.; Leriche, P.; Blanchard, P. *Adv. Mater.* **2014**, *26*, 3821−3838.
(29) Ni, W.; Wan, X.; Li, M.; Wang, Y.; Chen, Y. *Chem. Commun.* **2015**, *51*, 4936−4950.
(30) Lin, Y.; Zhan, X. *Acc. Chem. Res.* **2016**, *49*, 175−183.
(31) Sun, D.; Meng, D.; Cai, Y.; Fan, B.; Li, Y.; Jiang, W.; Huo, L.; Sun, Y.; Wang, Z. *J. Am. Chem. Soc.* **2015**, *137*, 11156−11162.
(32) Bura, T.; Leclerc, N.; Fall, S.; Lévêque, R.; Heiser, T.; Retailleau, P.; Rihn, S.; Mirloup, A.; Ziessel, R. *J. Am. Chem. Soc.* **2012**, *134*, 17404−17407.
(33) Bürckstummer, H.; Tulyakova, E. V.; Deppisch, M.; Lenze, N. M.; Kronenberg, M. R.; Gsänger, M.; Stolte, M.; Meerholz, K.; Würthner, F. *Angew. Chem., Int. Ed.* **2011**, *50*, 11628−11632.
(34) Xiao, X.; Wei, G.; Wang, S.; Zimmerman, J. D.; Renshaw, C. K.; Thompson, M. E.; Forrest, S. R. *Adv. Mater.* **2012**, *24*, 1956−1960.
(35) Liu, J.; Sun, Y.; Moonsin, P.; Kuik, M.; Proctor, C. M.; Lin, J.; Hsu, B. B.; Promarak, V.; Heeger, A. J.; Nguyen, T.-Q. *Adv. Mater.* **2013**, *25*, 5898−5903.
(36) Lim, N.; Cho, N.; Paek, S.; Kim, C.; Lee, J. K.; Ko, J. *Chem. Mater.* **2014**, *26*, 2283−2288.
(37) Gao, H.; Li, Y.; Wang, L.; Ji, C.; Wang, Y.; Tian, W.; Yang, X.; Yin, L. *Chem. Commun.* **2014**, *50*, 10251−10254.
(38) Wessendorf, C. D.; Schulz, G. L.; Mishra, A.; Kar, P.; Ata, I.; Weidelener, M.; Urdanpilleta, M.; Hanisch, J.; Mena-Osteritz, E.; Lindén, M.; Ahlswede, E.; Bäuerle, P. *Adv. Energy Mater.* **2014**, *4*, 1400266.
(39) Moon, M.; Walker, B.; Lee, J.; Park, S. Y.; Ahn, H.; Kim, T.; Lee, T.; Heo, H.; Seo, J. J. H.; Shin, T. J.; Kim, J. Y.; Yang, C. *Adv. Energy. Mater.* **2015**, *5*, 1402044.
(40) Tang, A.; Zhan, C.; Yao, J. *Chem. Mater.* **2015**, *27*, 4719−4730.
(41) Zhen, Y.; Tanaka, H.; Harano, K.; Okada, S.; Matsuo, Y.; Nakamura, E. *J. Am. Chem. Soc.* **2015**, *137*, 2247−2252.
(42) Cheng, M.; Chen, C.; Yang, X.; Huang, J.; Zhang, F.; Xu, B.; Sun, L. *Chem. Mater.* **2015**, *27*, 1808−1814.
(43) Sun, Y.; Welch, G. C.; Leong, W. L.; Takacs, C. J.; Bazan, G. C.; Heeger, A. J. *Nat. Mater.* **2012**, *11*, 44−48.
(44) Love, J. A.; Nagao, I.; Huang, Y.; Kuik, M.; Gupta, V.; Takacs, C. J.; Coughlin, J. E.; Qi, L.; van der Poll, T. S.; Kramer, E. J.; Heeger, A. J.; Nguyen, T.-Q.; Bazan, G. C. *J. Am. Chem. Soc.* **2014**, *136*, 3597−3606.
(45) Liu, X.; Sun, Y.; Hsu, B. B. Y.; Lorbach, A.; Qi, L.; Heeger, A. J.; Bazan, G. C. *J. Am. Chem. Soc.* **2014**, *136*, 5697−5708.
(46) Chen, X.; Liu, X.; Burgers, M. A.; Huang, Y.; Bazan, G. C. *Angew. Chem., Int. Ed.* **2014**, *53*, 14378−14381.
(47) Liu, Y.; Wan, X.; Wang, F.; Zhou, J.; Long, G.; Tian, J.; Chen, Y. *Adv. Mater.* **2011**, *23*, 5387−5391.
(48) Li, Z.; He, G.; Wan, X.; Liu, Y.; Zhou, J.; Long, G.; Zuo, Y.; Zhang, M.; Chen, Y. *Adv. Energy. Mater.* **2012**, *2*, 74−77.
(49) Zhou, J.; Wan, X.; Liu, Y.; Zuo, Y.; Li, Z.; He, G.; Long, G.; Ni, W.; Li, C.; Su, X.; Chen, Y. *J. Am. Chem. Soc.* **2012**, *134*, 16345−16351.
(50) Intemann, J. J.; Yao, K.; Ding, F.; Xu, Y.; Xin, X.; Li, X.; Jen, A. K.-Y. *Adv. Funct. Mater.* **2015**, *25*, 4889−4897.
(51) Qin, H.; Li, L.; Guo, F.; Su, S.; Peng, J.; Cao, Y.; Peng, X. *Energy Environ. Sci.* **2014**, *7*, 1397−1401.
(52) Gevaerts, V. S.; Herzig, E. M.; Kirkus, M.; Hendriks, K. H.; Wienk, M. M.; Perlich, J.; Müller-Buschbaum, P.; Janssen, R. A. J. *Chem. Mater.* **2014**, *26*, 916−926.
(53) Yu, Q.-C.; Fu, W.-F.; Wan, J.-H.; Wu, X.-F.; Shi, M.-M.; Chen, H.-Z. *ACS Appl. Mater. Interfaces* **2014**, *6*, 5798−5809.
(54) Park, Y. S.; Kale, T. S.; Nam, C.-Y.; Choi, D.; Grubbs, R. B. *Chem. Commun.* **2014**, *50*, 7964−7967.
(55) Shin, W.; Yasuda, T.; Hidaka; Watanabe, Y. G.; Arai, R.; Nasu, K.; Yamaguchi, T.; Murakami, W.; Makita, K.; Adachi, C. *Adv. Energy. Mater.* **2014**, *4*, 1400879.
(56) Yin, Q.-R.; Miao, J.-S.; Wu, Z.; Chang, Z.-F.; Wang, J.-L.; Wu, H.-B.; Cao, Y. *J. Mater. Chem. A* **2015**, *3*, 11575−11586.
(57) Wang, J.-L.; Wu, Z.; Miao, J.-S.; Liu, K.-K.; Chang, Z.-F.; Zhang, R.-B.; Wu, H.-B.; Cao, Y. *Chem. Mater.* **2015**, *27*, 4338−4348.
(58) Lin, Y.; He, Q.; Zhao, F.; Huo, L.; Mai, J.; Lu, X.; Su, C.-J.; Li, T.; Wang, J.; Zhu, J.; Sun, Y.; Wang, C.; Zhan, X. *J. Am. Chem. Soc.* **2016**, *138*, 2973−2976.
(59) Zhou, J.; Zuo, Y.; Wan, X.; Long, G.; Zhang, Q.; Ni, W.; Liu, Y.; Li, Z.; He, G.; Li, C.; Kan, B.; Li, M.; Chen, Y. *J. Am. Chem. Soc.* **2013**, *135*, 8484−8487.
(60) Yuan, L.; Zhao, Y.; Zhang, J.; Zhang, Y.; Zhu, L.; Lu, K.; Yan, W.; Wei, Z. *Adv. Mater.* **2015**, *27*, 4229−4233.
(61) Gupta, V.; Kyaw, A. K. K.; Wang, D. H.; Chand, S.; Bazan, G. C.; Heeger, A. J. *Sci. Rep.* **2013**, *3*, 1965.

DOI: 10.1021/jacs.6b03495
J. Am. Chem. Soc. 2016, 138, 7687−7697

(62) Kyaw, A. K. K.; Wang, D. H.; Wynands, D.; Zhang, J.; Nguyen, T.-Q.; Bazan, G. C.; Heeger, A. J. *Nano Lett.* **2013**, *13*, 3796−3801.
(63) Gao, K.; Li, L.; Lai, T.; Xiao, L.; Huang, Y.; Huang, F.; Peng, J.; Cao, Y.; Liu, F.; Russell, T. P.; Janssen, R. A. J.; Peng, X. *J. Am. Chem. Soc.* **2015**, *137*, 7282−7285.
(64) Duan, C.; Furlan, A.; van Franeker, J. J.; Willems, R. E. M.; Wienk, M. M.; Janssen, R. A. J. *Adv. Mater.* **2015**, *27*, 4461−4468.
(65) Liu, Y.; Chen, C.-C.; Hong, Z.; Gao, J.; Yang, Y.; Zhou, H.; Dou, L.; Li, G.; Yang, Y. *Sci. Rep.* **2013**, *3*, 3356.
(66) Kan, B.; Li, M.; Zhang, Q.; Liu, F.; Wan, X.; Wang, Y.; Ni, W.; Long, G.; Yang, X.; Feng, H.; Zuo, Y.; Zhang, M.; Huang, F.; Cao, Y.; Russell, T. P.; Chen, Y. *J. Am. Chem. Soc.* **2015**, *137*, 3886−3893.
(67) Kan, B.; Zhang, Q.; Li, M.; Wan, X.; Ni, W.; Long, G.; Wang, Y.; Yang, X.; Feng, H.; Chen, Y. *J. Am. Chem. Soc.* **2014**, *136*, 15529−15532.
(68) Sun, K.; Xiao, Z.; Lu, S.; Zajaczkowski, W.; Pisula, W.; Hanssen, E.; White, J. M.; Williamson, R. M.; Subbiah, J.; Ouyang, J.; Holmes, A. B.; Wong, W. W. H.; Jones, D. J. *Nat. Commun.* **2015**, *6*, 6013.
(69) Cui, C.; Guo, X.; Min, J.; Guo, B.; Cheng, X.; Zhang, M.; Brabec, C. J.; Li, Y. *Adv. Mater.* **2015**, *27*, 7469−7475.
(70) Liu, X.; Hsu, B. B. Y.; Sun, Y.; Mai, C.-K.; Heeger, A. J.; Bazan, G. C. *J. Am. Chem. Soc.* **2014**, *136*, 16144−16147.
(71) Liu, X.; Sun, Y.; Hsu, B. B. Y.; Lorbach, A.; Qi, L.; Heeger, A. J.; Bazan, G. C. *J. Am. Chem. Soc.* **2014**, *136*, 5697−5708.
(72) Zhou, C.; Liang, Y.; Liu, F.; Sun, C.; Huang, X.; Xie, Z.; Huang, F.; Roncali, J.; Russell, T. P.; Cao, Y. *Adv. Funct. Mater.* **2014**, *24*, 7538−7547.
(73) Wang, N.; Chen, Z.; Wei, W.; Jiang, Z. *J. Am. Chem. Soc.* **2013**, *135*, 17060−17068.
(74) Park, J. H.; Jung, E. H.; Jung, J. W.; Jo, W. H. *Adv. Mater.* **2013**, *25*, 2583−2588.
(75) Li, W.; Albrecht, S.; Yang, L.; Roland, S.; Tumbleston, J. R.; McAfee, T.; Yan, L.; Kelly, M. A.; Ade, H.; Neher, D.; You, W. *J. Am. Chem. Soc.* **2014**, *136*, 15566−15576.
(76) Yum, S.; An, T. K.; Wang, X.; Lee, W.; Uddin, M. A.; Kim, Y. J.; Xu, T. L.; Nguyen, S.; Hwang, S.; Park, C. E.; Woo, H. Y. *Chem. Mater.* **2014**, *26*, 2147−2154.
(77) Zhang, M.; Guo, X.; Zhang, S.; Hou, J. *Adv. Mater.* **2014**, *26*, 1118−1123.
(78) Deng, Y.; Liu, J.; Wang, J.; Liu, L.; Li, W.; Tian, H.; Zhang, X.; Xie, Z.; Geng, Y.; Wang, F. *Adv. Mater.* **2014**, *26*, 471−476.
(79) Lei, T.; Xia, X.; Wang, J.-Y.; Liu, C.-J.; Pei, J. *J. Am. Chem. Soc.* **2014**, *136*, 2135−2141.
(80) Fei, Z.; Boufflet, P.; Wood, S.; Wade, J.; Moriarty, J.; Gann, E.; Ratcliff, E. L.; McNeill, C. R.; Sirringhaus, H.; Kim, J.-S.; Heeney, M. *J. Am. Chem. Soc.* **2015**, *137*, 6866−6879.
(81) Dou, L.; Chen, C.-C.; Yoshimura, Y.; Ohya, K.; Chang, W.-H.; Gao, J.; Liu, Y.; Richard, E.; Yang, Y. *Macromolecules* **2013**, *46*, 3384.
(82) Wang, J.-L.; Yin, Q.-R.; Miao, J.-S.; Wu, Z.; Chang, Z.-F.; Cao, Y.; Zhang, R.-B.; Wang, J.-Y.; Wu, H.-B.; Cao, Y. *Adv. Funct. Mater.* **2015**, *25*, 3514−3523.
(83) Li, M.; Liu, F.; Wan, X.; Ni, W.; Kan, B.; Feng, H.; Zhan, Q.; Yang, X.; Wang, Y.; Zhang, Y.; Shen, Y.; Russell, T. P.; Chen, Y. *Adv. Mater.* **2015**, *27*, 6296−6302.
(84) Schulz, G. L.; Löbert, M.; Ata, I.; Urdanpilleta, M.; Lindén, M.; Mishra, A.; Bäuerle, P. *J. Mater. Chem. A* **2015**, *3*, 13738−13748.
(85) Ni, W.; Li, M.; Liu, F.; Wan, X.; Feng, H.; Kan, B.; Zhang, Q.; Zhang, H.; Chen, Y. *Chem. Mater.* **2015**, *27*, 6077−6084.
(86) Sun, K.; Xiao, Z.; Hanssen, E.; Klein, M. F. G.; Dam, H. H.; Pfaff, M.; Gerthsen, D.; Wong, W. W. H.; Jones, D. J. *J. Mater. Chem. A* **2014**, *2*, 9048−9054.
(87) Zhang, M.; Guo, X.; Wang, X.; Wang, H.; Li, Y. *Chem. Mater.* **2011**, *23*, 4264−4270.
(88) Bai, H.; Wang, Y.; Cheng, P.; Li, Y.; Zhu, D.; Zhan, X. *ACS Appl. Mater. Interfaces* **2014**, *6*, 8426−8433.
(89) Liu, D.; Xiao, M.; Du, Z.; Yan, Y.; Han, L.; Roy, V. A. L; Sun, M.; Zhu, W.; Lee, C. S.; Yang, R. *J. Mater. Chem. C* **2014**, *2*, 7523−7530.
(90) Bronstein, H.; Frost, J. M.; Hadipour, A.; Kim, Y.; Nielsen, C. B.; Ashraf, R. S.; Rand, B. P.; Watkins, A.; McCulloch, I. *Chem. Mater.* **2013**, *25*, 277−285.
(91) Liu, X.; Li, Q.; Li, Y.; Gong, X.; Su, S.-J.; Cao, Y. *J. Mater. Chem. A* **2014**, *2*, 4004−4013.
(92) Wang, J.-L.; Xiao, F.; Yan, J.; Wu, Z.; Liu, K.-K.; Chang, Z.-F.; Zhang, R.-B.; Chen, H.; Wu, H.-B.; Cao, Y. *Adv. Funct. Mater.* **2016**, *26*, 1803−1812.
(93) Wei, G.; Wang, S.; Sun, K.; Thompson, M. E.; Forrest, S. R. *Adv. Energy. Mater.* **2011**, *1*, 184−187.
(94) Huang, Y.; Kramer, E.; Heeger, A. J.; Bazan, G. C. *Chem. Rev.* **2014**, *114*, 7006−7043.
(95) Mukherjee, S.; Proctor, C. M.; Tumbleston, J. R.; Bazan, G. C.; Nguyen, T.-Q.; Ade, H. *Adv. Mater.* **2015**, *27*, 1105−1111.
(96) Liu, F.; Wang, C.; Baral, J. K.; Zhang, L.; Watkins, J. J.; Briseno, A. L.; Russell, T. P. *J. Am. Chem. Soc.* **2013**, *135*, 19248−19259.
(97) Proctor, C. M.; Love, J. A.; Nguyen, T.-Q. *Adv. Mater.* **2014**, *26*, 5957−5961.
(98) Yang, D.; Yang, L.; Huang, Y.; Jiao, Y.; Igarashi, T.; Chen, Y.; Lu, Z.; Pu, X.; Sasabe, H.; Kido, J. *ACS Appl. Mater. Interfaces* **2015**, *7*, 13675−13684.
(99) Bull, T. A.; Pingree, L. S. C.; Jenekhe, S. A.; Ginger, D. S.; Luscombe, C. L. *ACS Nano* **2009**, *3*, 627−636.
(100) Kwon, O. K.; Park, J.-H.; Kim, D. W.; Park, S. K.; Park, S. Y. *Adv. Mater.* **2015**, *27*, 1951−1956.

DOI: 10.1021/jacs.6b03495
J. Am. Chem. Soc. 2016, 138, 7687−7697